International Journal of Automotive Technology, Vol. 7, No. 7, pp. 867–872 (2006)

1229–9138/2006/031–15

SIMULATION OF UNIT CELL PERFORMANCE IN THE POLYMER ELECTROLYTE MEMBRANE FUEL CELL

H. G. KIM[1)*], Y. S. KIM[1)] and Z. SHU[1,2)]

[1)]Department of Mechanical and Automotive Engineering, Jeonju University, Jeonju 560-759, Korea
[2)]Shanghai Institute of Applied Mathematics and Mechanics, Shanghai University, Shanghai 200072, China

(Received 2 August 2005; Revised 5 September 2006)

ABSTRACT–Fuel cells are devices that convert chemical energy directly into electrical energy. Owing to the high efficiency of the fuel cells, a large number of research work have been done during these years. Among many kinds of the fuel cells, a polymer electrolyte membrane fuel cell is such kind of thing which works under low temperature. Because of the specialty, it stimulated intense global R&D competition. Most of the major world automakers are racing to develop polymer electrolyte membrane fuel cell passenger vehicles. Unfortunately, there are still many problems to be solved in order to make them into the commercial use, such as the thermal and water management in working process of PEMFCs. To solve the difficulites facing the researcher, the analysis of the inner mechanism of PEMFC should be implemented as much as possible and mathematical modeling is an important tool for the research of the fuel cell especially with the combination of experiment. By regarding some of the assumptions and simplifications, using the finite element technique, a two-dimensional electrochemical mode is presented in this paper for the further comparison with experimental data. Based on the principals of the problem, the equations of electronic charge conservation equation, gas-phase continuity equation, and mass balance equation are used in calculating. Finally, modeling results indicate some of the phenomenon in a unit cell, and the relationships between potential and current density.

KEY WORDS : PEMFC, Current density, Potential, Numerical simulation, Mass fraction, Hydrogen, Oxygen, Water

1. INTRODUCTION

During the past decade, fuel cell has stimulated with intense global R&D competition. The largest part of research efforts has been devoted to the development of kW-scale applications on the electric vehicles driven by fuel cell, which results that most of the major world automakers are racing to develop fuel cell passenger vehicles. On the other hand, small fuel cells, which can take the place of the traditional batteries in such portable electronic devices as mobile phones, laptop, palmtop and solar hydrogen systems (Bernardi and Verbrugge, 1991; Dyer, 2002; Meyers and Haynard, 2002; Raadschelders and Jansen, 2001; Heinze *et al.*, 2002), has been received increasing interest. Among many kinds of fuel cells, the polymer electrolyte membrane fuel cell, the PEMFC, named by its polymer electrolyte membrane, is usually regarded as the most promising fuel cell type for the applications. Compared to typical batteries, fuel cell, having characteristics similar to them although, differs in several respects. For example, battery is an energy storage device, with the maximum available energy determined by the amount of chemical reactant stored in the battery; while, the fuel cell, is a device which converts chemical energy directly into electrical energy and stands for longer operating times and fast refueling, when comparing with the traditional battery. At the same time fuel cells are more sensitive to impurities in fuel and air comparing to traditional battery. In addition, the environmental effect of discarded batteries is regarded as a problem, but the waste products of fuel-cell reactions are water and heat. Unfortunately, fuel cell is not mature enough to compete with established battery technologies (Yang, 2000), the cost of fuel cells still remains high and unaffordable for most of the consumers, and very few products are available with full commercial warranties and a track record for reliable operation. Other barriers to commerial use are as following: fuel cell cost, fuel cell durability, fuel infrastructure, and hydrogen storage. As to the PEMFC, thermal and water management is important (Fuller and Newman, 1993; Yi and Nguyen, 1999; He *et al.*, 2000), because PEMFC is operated and effected at relatively low temperature (Gurski and Nelson, 2003), around 330–350 K, and require humidification of the air and fuel supplies to prevent performance degradation. In order to analyze and solve the problems above,

*Corresponding author. e-mail: hkim@jj.ac.kr

the way of using numerical simulation and experiment with alternative materials, is one of the recommended method to improve the cell-channel design because the experiment can serve first to guide and validate models and allow parameters to be fit, and then, models of simulation can identify critical parameters that will be the subject of experimental measurement or the target for materials engineering (Yi, 1998; Marr and Li, 2000), Thus, to increase full-cell reliability and durability of the experiment model, the numerical simulation model is created in this paper, in the end, the comparison is implemented according to the simulation results and experimental data.

2. MODEL AND WORKING PRINCIPLE

The PEMFC model is composed of three domains: Anode, Proton exchange membrane, and Cathode, as in indicated in Figure 1, each of the porous electrodes is in contact with an interdigitated gas distributor, which has a inlet channel, a current collector, and an outlet channel. hydrogen is feeded into the channel of the anode, at the same time, humidified air is feeded into the cathode. At the anodic, hydrogen reacts and is consumed active layer to form protons that carries the ionic current to the cathode, at the cathode, oxygen reacts the protons to form water, at the active layer like this way:

$$H_2 \rightarrow 2H^+ + 2e^- \quad \text{at Anode} \tag{1}$$

$$O_2 + 4H^+ + 4e^- \rightarrow 2H_2O \quad \text{at Cathode} \tag{2}$$

The maximum theoretical efficiency is not bound by the Carnot cycle, when converting chemical energy to electrical energy directly, PEMFC typically achieve fuel efficiencies as high as 50%, which is more efficient than the other ways (Kim *et al.*, 2004). So it is very attractive in automobile applications.

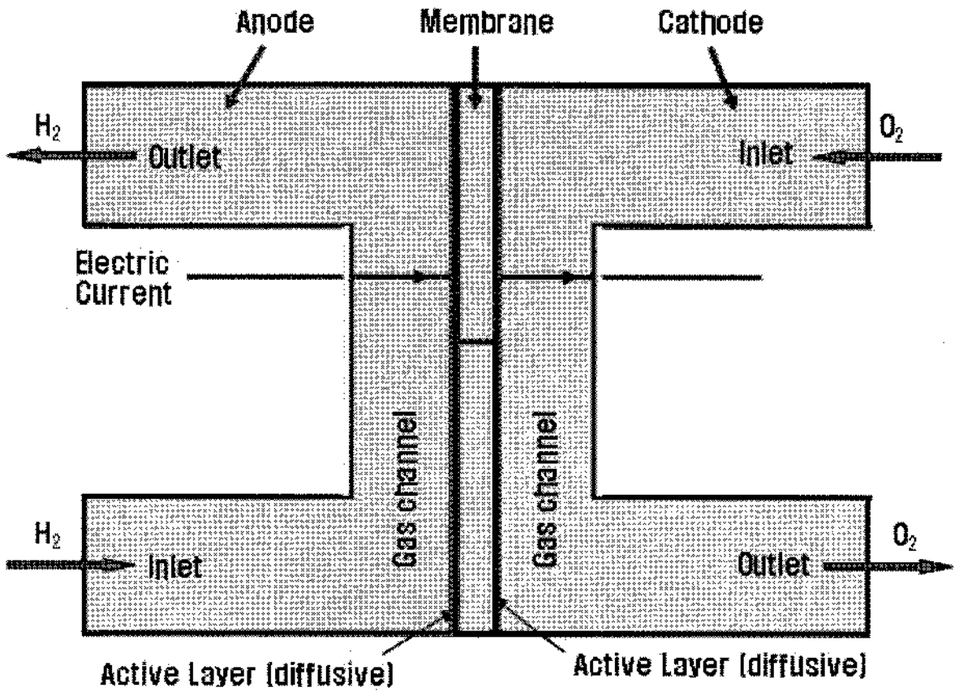

Figure 1. The explanation of the PEMFC working principle.

3. GOVERNING EQUATIONS

Current balance, mass balance, and momentum balance are used in the model to simulate the behavior of the PEMFC (Comsol 3.1, 2003). The potential distribution is modeled in three subdomains, which is given by following equations

$$\nabla \cdot (-\kappa^{s,\,eff} \nabla \phi_s) = 0 \quad \text{at Anode} \tag{3}$$

$$\nabla \cdot (-\kappa^{m,\,eff} \nabla \phi_m) = 0 \quad \text{at Membrane} \tag{4}$$

$$\nabla \cdot (-\kappa^{s,\,eff} \nabla \phi_s) = 0 \quad \text{at Cathode} \tag{5}$$

where $\kappa^{m,\,eff}$ is the effective conductivity (S/m) which is generally a function of relative humidity. However, it is fixed as the value of 9 S/m assuming at 100% relative humidity condition to investigate the general physical phenomena. The potential (V) in the electrode phases are denoted by ϕ_s, while in the membrane it is denoted by ϕ_m.

Within the electrodes' pores, the gas-phase is considered as a continuous phase and, thus, its momentum conservation equation can be represented using the Darcy's law.

$$u = -k_p \nabla p / \eta \tag{6}$$

Where, k_p denoted the permeability (m^2) of the electrode, η denoted the viscosity (kg/m/s) of the gas and p denoted the pressure (Pa).

Maxwell-Stefan Diffusion and Convention equation is used in anode and cathode respectively, for the former H_2, H_2O are considered; for the latter, the O_2, H_2O, and N_2 are considered.

$$\frac{\partial}{\partial t}\rho\omega_i + \nabla\left[-\rho\omega_i \sum_{j=1}^{N} D_{ij}A + \omega_i \rho u + D_i^T \frac{\nabla T}{T}\right] = R_i \tag{7}$$

where

$$A = \left\{ \frac{M}{M_j}\left(\nabla\omega_j + \omega_j \frac{\nabla M}{M}\right) + (x_j - \omega_j)\frac{\nabla p}{p} \right\}$$

T is the temperature (K), u is the velocity (ms^{-1}) of fluids, x is mole fraction, ω is mass fraction, M is the mole masses (kg mol^{-1}), D_{ij} is the diffusion coefficient (m^2s^{-1}), D_i^T is the transpose of the diffusion coefficient matrix, R_i is the velocity of reacting matters, p denoted the pressure (Pa), ρ is the density (kg m^{-3}), which is given to the equation $\rho = \sum_i x_i M_i$.

4. BOUNDARY CONDITIONS

4.1. Model Geometry

Based on the real geometry of the experiment, the model

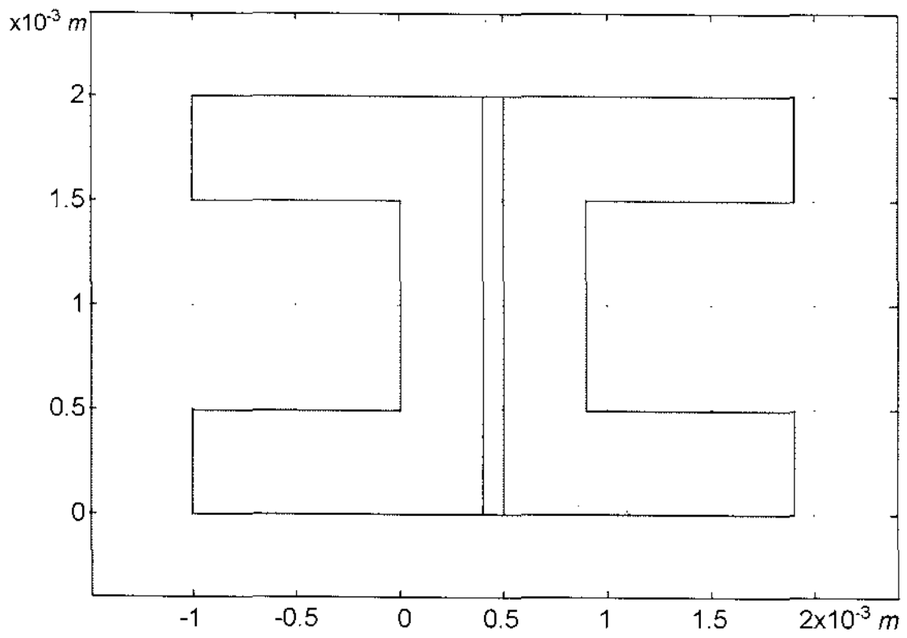

Figure 2. Geometry of the model.

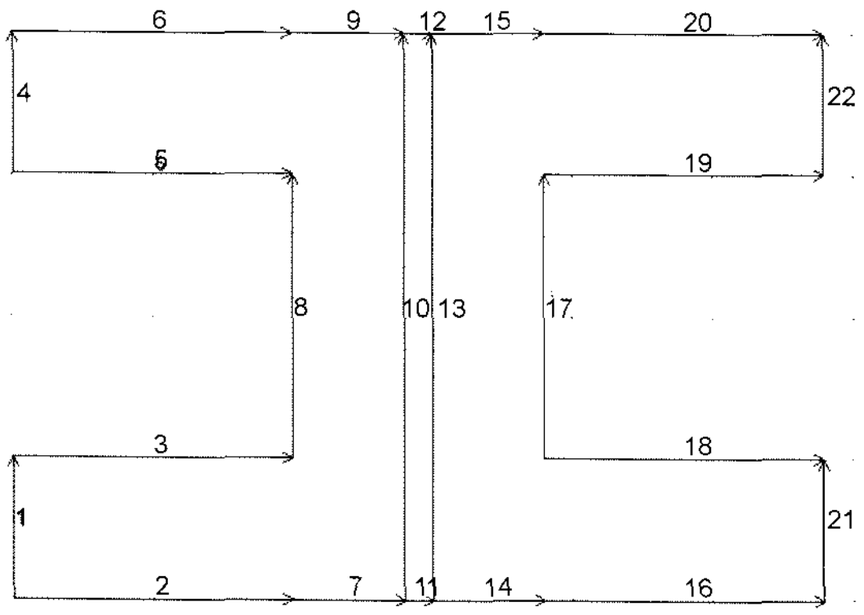

Figure 3. Boundary numbers of the PEMFC.

is presented here as shown in the Figure 2. The model is a unit cell repeating through the interdigitated channel. Here, electrode height is 2 mm, electrode width is 0.4 mm, membrane thickness is 0.1 mm, and collector height is 1 mm.

4.2. Boundary Conditions and Mesh Generation

Boundary conditions are specified here based on the linear physical properties. The upper and bottom line assumed to be left insulated. Line boundary condition No.10 (see Figure 3), which stands for the boundary condition for the current density at the interface between the anode and the membrane (Scott Forgler, 1999), can be written as:

$$(-\kappa^{s,\,eff}\nabla\phi_s)\cdot n=i_a \tag{8}$$

$$i_a=-K_1(c_{H_2}^{agg}-c_{H_2}^{ref}\exp(-K_2\cdot(\phi_s-\phi_m-\Delta\phi_{eq,\,a})))\cdot(1-K_3\coth K_3) \tag{9}$$

$$K_1=6\delta_l(1-\varepsilon)FD_{H_2}^{agg}/(R^{agg})^2 \tag{10}$$

$$K_2=2F/RT \tag{11}$$

$$K_3=\sqrt{i_{0,a}S/(2Fc_{H_2}^{ref}D_{H_2}^{agg})}R^{agg} \tag{12}$$

where δ_l is the active layer thickness with the value 1.0×10^{-5} m, $D_{H_2}^{agg}$ is the gas diffusive coefficient inside the agglomerate, R^{agg} is agglomerate particle radius 1.0×10^{-7} m, F is Faraday's constant with the value 96,487 As/mol, R is universal gas constant with the value 8.314 J/mol K, T is the temperature value 343 K, ϕ_a^{cc} is the potential at the anode current collector, with the value 0 V. On the other hand, ε is dry porosity of the electrodes with the value 0.4, S is specific surface area of the electrodes with the value 1.0×10^7 m^2/m^3, η is gas viscosity in the electrode's pores with the value 2.1×10^{-5} (Pa·sec).

Line boundary condition No.13 (see Figure 3.), which stands for the boundary condition for the current density at the interface between the cathode and the membrane, can be written as:

$$(-\kappa^{s,\,eff}\nabla\phi_s)\cdot n=i_c \tag{13}$$

$$i_c=K_4c_{O_2}^{agg}(1-\sqrt{K_4\exp(-K_6(\phi_s-\phi_m-\phi_{eq}^c))})\cdot\coth\cdot(\sqrt{K_5\exp(-K_6(\phi_s-\phi_m-\phi_{eq}^c))}) \tag{14}$$

$$K_4=12\delta_l(1-\varepsilon)FD_{O_2}^{agg}/(R^{agg})^2 \tag{15}$$

$$K_5=i_{0,c}S(R^{agg})^2/(4Fc_{O_2}^{ref}D_{O_2}^{agg}) \tag{16}$$

$$K_6=F/2RT \tag{17}$$

Concentration of the dissolved hydrogen and oxygen at the surface of the agglomerate particles are defined by the Henry's law:

$$c_{H_2}^{agg}=p_{H_2}y_{H_2}/H_{H_2} \tag{18}$$

$$c_{O_2}^{agg}=p_{O_2}y_{O_2}/H_{O_2} \tag{19}$$

where $c_{H_2}^{agg}$ is the agglomerate hydrogen concentration in the active layer, $y_{H_2,in}$ is molar fraction of hydrogen at the anode inlet with the value 0.6, $c_{O_2}^{agg}$ is the agglomerate oxygen concentration in the active layer, $y_{O_2,in}$ is molar fraction of oxygen at the cathode inlet with the value 0.21. On the other hand, H_{H_2} is Henry's concentration coefficient for hydrogen with the value 3.9×10^4 (Pa ·m^3/$mole^{-1}$), H_{O_2} is Henry's concentration coefficient for oxygen with the value 3.2×10^4 (Pa·m^3/mole).

The current density, normal to the membrane domain, which is at the interfaces between the electrodes and the membrane, is ruled by

$$(-\kappa^{m,\,eff}\nabla\phi_m)\cdot n=-i_a \tag{20}$$

$$(-\kappa^{m,\,eff}\nabla\phi_m)\cdot n=-i_c \tag{21}$$

The mass transfer of species across the anodic and cathodic active layers is also related to the local current density according to:

$$-n\cdot n_{H_2}=-\frac{i_a}{2F} \tag{22}$$

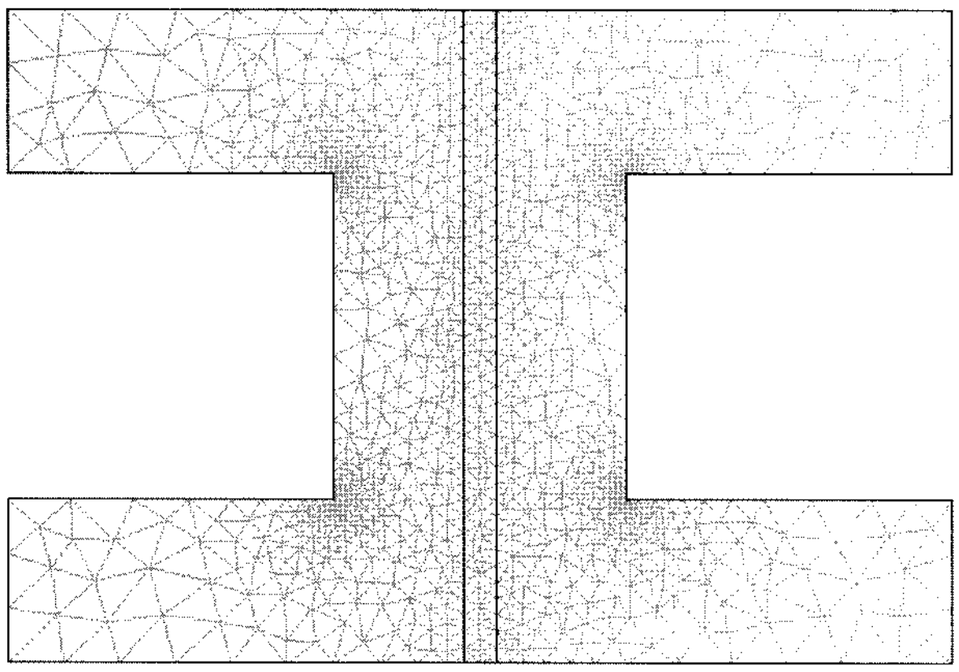

Figure 4. The created mesh of the model.

$$-n \cdot n_{O_2} = -\frac{i_c}{4F} \tag{23}$$

$$-n \cdot n_{H_2O} = d_{H_2O}\frac{i_c}{F} \tag{24}$$

Where d_{H_2O} is the drag factor of water. Assuming that hydrogen proton carries water particle of three, d_{H_2O}, 3 is used. At the remaining boundaries it is applied to insulated or symmetric conditions.

The potential at the anode current collector is set as $\phi_s = 0$, cathode is set as $\phi_s = V_{cell}$, where V_{cell} is the potential at the cathode current collector, with the value 0.7 V. The gas pressure of the inlet and outlet is set as following: $p = p_{a,in}$, $p = p_{c,in}$, $p = p_{ref}$.

Where $p_{a,in}$ is the gas pressure at the anode inlet with the value $p_0 \times 1.1$, $p_{c,in}$ are the gas pressure at the cathode inlet with the value $p_0 \times 1.1$, $p_{a,out}$ is the gas pressure at the anode outlet with the value p_0, $p_{c,out}$, is the gas pressure at the cathode outlet with the value p_0.

The finite element meshes are generated under the boundary condition as shown in Figure 4. Hence, the element growth rate is 1.3, mesh curvature factor is 0.3, mesh curvature cut off is 0.001, the number of the element is 9,016, number of boundary element is 456.

5. RESULTS AND DISCUSSION

Based on the governing equation and boundary condition, simulation results are described from Figure 5 to 10. Figure 5 shows current density distribution and current field (arrow plot) in the fuel cell operating at 0.7 V. The current density increases from the center to the edges of the current collectors, this results in the variation of hydrogen velocity's along the gas channel.

Figure 6 shows the current density at the active layer is plotted as a function of fuel cell height (y). The current density is different according to the Are-length, the highest current density is presented in the uppest region of the PEMFC with its value 3,075 A/m^2. This means the current density is heavily depended on the oxygen reduction reaction rate in the cathode. Figure 7 shows the

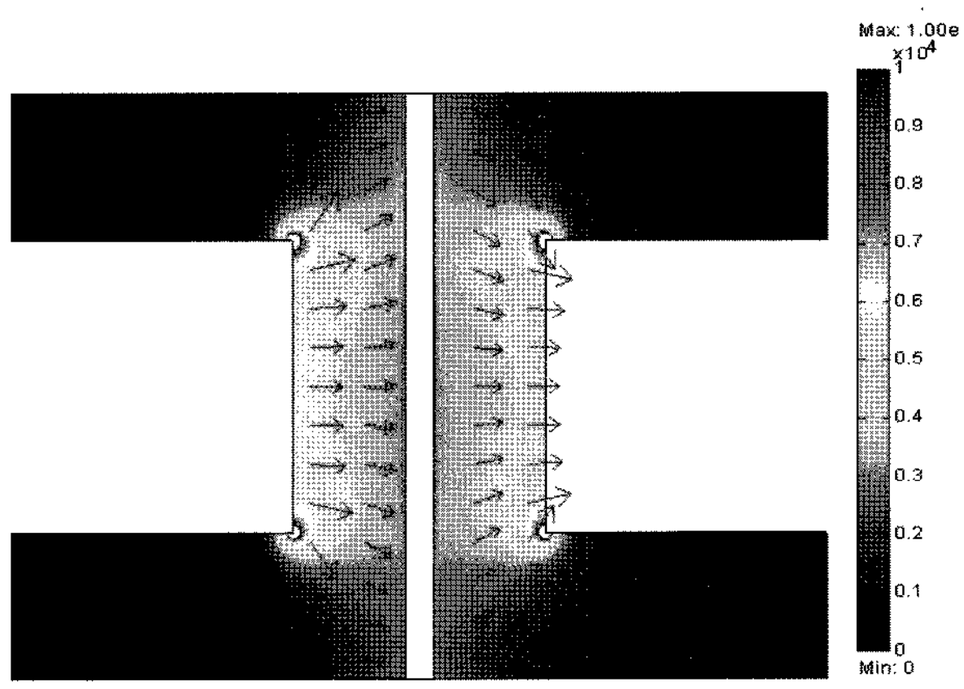

Figure 5. Current density distribution and current field (arrow plot) in the fuel cell operating at 0.7 V, the anode and the cathode is on the left and right respectively.

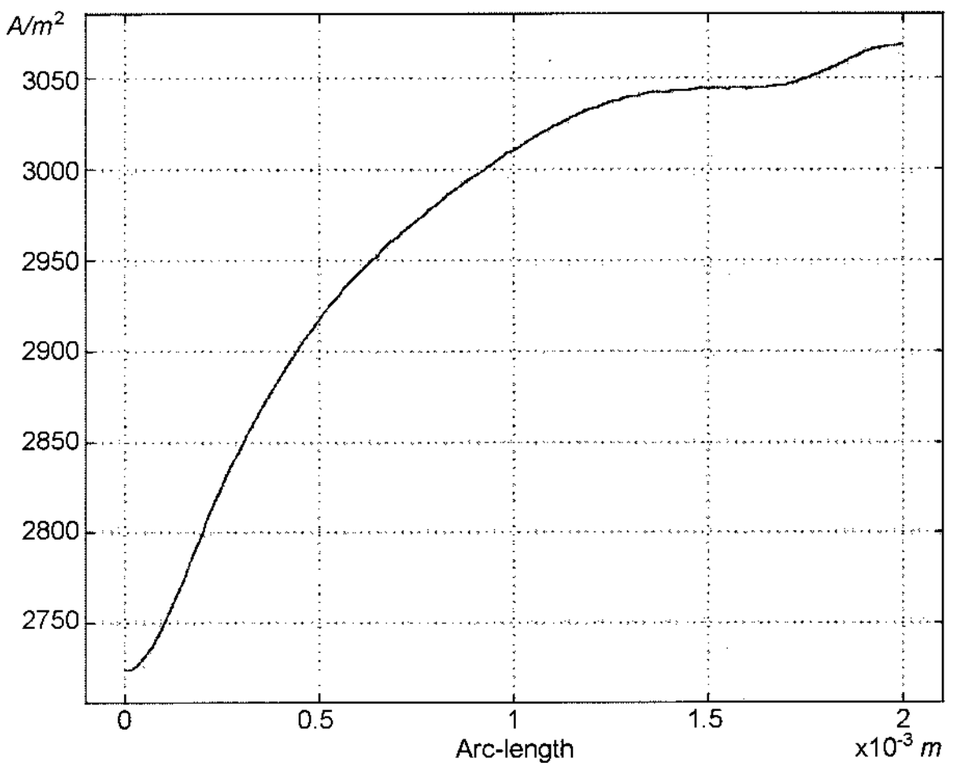

Figure 6. The current density at the active layer.

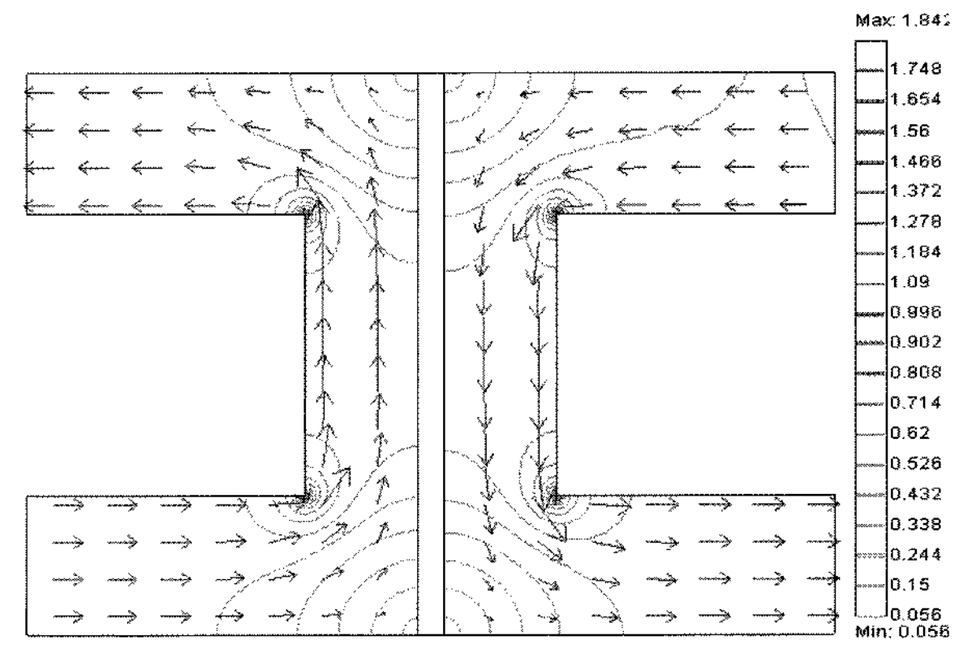

Figure 7. Hydrogen and oxygen velocity (m/s) distribution and direction in the anode and cathode respectively.

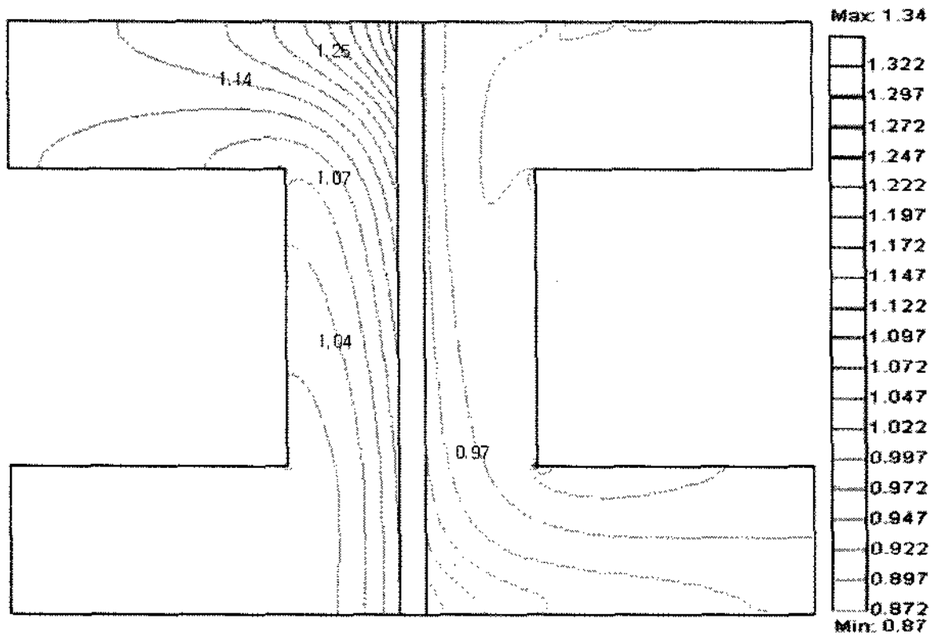

Figure 8. Reactant mass fraction, which is normalized by its inlet value, hydrogen is the reactant on the anode side (left), and oxygen on the cathode side (right).

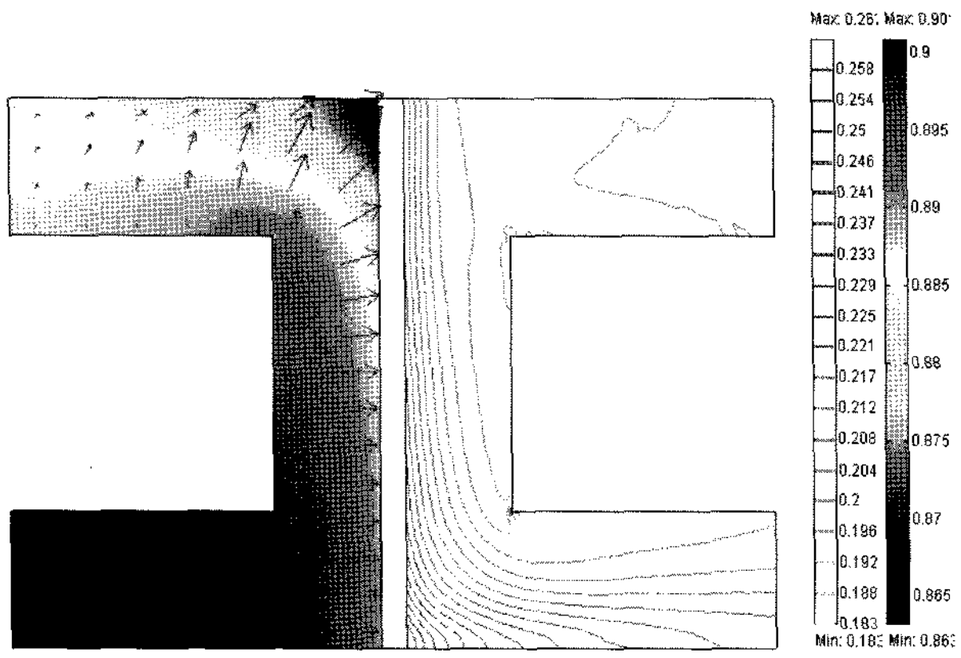

Figure 9. Fraction of water in the anode (left part) and cathode (right part). The color plot shows the mass fraction of the water in the anode, while the contour plot shows the mass fractions of water in the cathode. The arrow plot shows the diffusive flux vector leaving the anode side.

hydrogen and oxygen velocity distribution and direction in the anode and cathode respectively. The even velocity (about 1.1 m/s) distribution along the active layer means the strong convective flux in the gas backing. The velocity difference between the maximun and minimun is 1.69 m/s. Figure 8 shows the reactant mass fraction, which is normalized by its inlet value, The hydrogen mass fraction increase along the period from the inlet to the outlet, which means the drag induced flux of water is higher than the hydrogen consumption; while, in the cathode, the oxygen mass fraction varies little because of the stoichiometric excess in the inlet of the cathode. Figure 9 shows the fraction of water in the anode (left part) and cathode (right part). The color plot shows the mass fraction of the water in the anode, while the contour plot shows the mass fractions of water in the cathode.

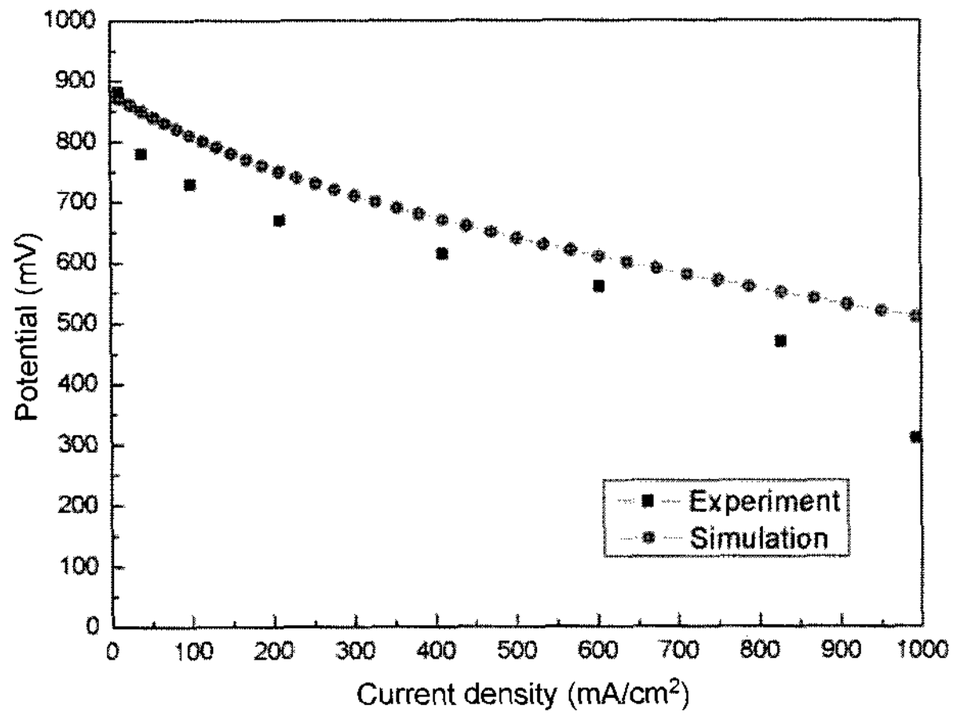

Figure 10. Comparison of the simulation result and experiment data.

The arrow plot shows the diffusive flux vector leaving the anode side. Water is transported through the way of convection and also the way of diffusion to the membrane on the anode side. The water fraction decreases along the way the gas passes, which deduces the limitation of the PEMFC performance.

Figure 10 shows V-I performance curve which presents comparison of the simulation result and experiment data. The experiment is implemented under pressure of 1.1 atm and humidification. The amount of the hydrogen and oxygen as a fuel is fixed at 60 sccm in anode and 40 sccm in cathode where the cell temperature is set 343 K (70°C). The inclination of the simulation and the experiment are almost same, the largest difference exists in the concentration polarization zone. The discrepancy of the simulation and the experiment results in the zone from 0 to 800 (mA/cm^2) is no more than 100 mV. During the zone from 800 to 1000 (mA/cm^2), the discrepancy began to increase when comparing the zone from 0 to 800 (mA/cm^2) according to exponentially decrease in analysis result.

6. CONCLUSIONS

A 2-D finite element model for a PEMFC, together with experiments using a unit cell comprising interdigitated flow fields, has been considered. The model, which takes into account two-dimentional flow of momentum, current and mass on the cathode side, as well as conservation of charge throughout the whole cell, is implemented with corresponding measurements in the serpentine unit cell. Special attention is given to ensure that the measurements are conducted under conditions similar to the model.

The model presents the promising curve which is sufficient for between simulation and experiment. It is shown, however, that under the concentration polarization

zone this simulation of fuel cell has some discrepancy comparing to the experiment. It is due to the result that the formulation of the fuel cell is not considered concentration effect as calibration factor. It is found that the repeated cost-loss could be saved because even fuel cell for the stack gives the reasonable results.

In further studies, the measurement condition will be chosen for investigations of the influence of the temperature and of the mass fraction in PEMFC. Furthermore, the stack analysis will be performed through simulations in which the current density measurements are used for validation of the models.

ACKNOWLEDGEMENT–This research was supported by the program of New & Renewable Energy Center of Korea Energy Management Corporation and the Program for the Training of Graduate Students in Regional Innovation which was conducted by the Ministry of Commerce, Industry and Energy of the Korean Government.

REFERENCES

Bernardi, D. M. and Verbrugge, M. W. (1991). Mathematical model of a gas diffusion electrode bonded to a polymer electrolyte. *AIChe J.*, **37**, 1151–1163.

Comsol 3.1 (2003). *Comsol Multiphysics Manual.* Burlington. MA. USA.

Dyer, C. K. (2002). Fuel cells for portable applications. *J. Power Sources,* **106**, 31–34.

Fuller, T. F. and Newman, J. (1993). Water and thermal management in solid-polymer-electolyte fuel Cells. *J. Electrochem. Soc.*, **140**, 1218.

Gurski, S. D. and Nelson, D. J. (2003). Cold start fuel economy and power limitations for a PEM fuel cell vehicle. *SAE Paper No.* 2003-01-0422.

He, W., Yi, J. S. and Nguyen, T. V. (2000). Two-phase flow model of the cathode of PEM fuel cells using interdigitated flow field. *AIChe J.,* **46**, 2053.

Heinzel, C., Hebling, M., Muller, M., Zedda, M. and Muller, C. (2002). Fuel cells for low power applications. *J. Power Sources* **2, 105**, 250–255.

Kim, H. G., Nah, S. C., Kim, S. C., Kang, Y. W., Yang, G. E., Lee, H. K. and Choi, M. C. (2004). A study on the dynamic analysis in the shaft of tubro-blower for fuel cell. *J. Korean Soc. for Machine Tool Engineers,* **13,** 81–87.

Meyers, J. P. and Maynard, H. L. (2002). Design considerations for miniaturized PEM fuel cells. *J. Power Sources,* **109**, 76–88.

Marr, C. and Li, X. (2000). Two-dimensional finite element method study of the resistance of membranes in polymer electrolyte fuel cells. *Electrochimica Acta,* **45**, 1741–1751.

Raadschelders, J. W. and Jansen, T. (2001). Energy sources for the future dismounted soldier, the total integration of the energy consumption within the soldier system. *J. Power Sources,* **96**, 160–166.

Scott Fogler, H. (1999). *Element of Chemical Reaction Engineering*. 3rth edn.

Yi, J. S. and Nguyen, T. V. (1998). An along the channel model for PEMFC. *J. Electrochem. Soc.*, **145**, 1149.

Yi, J. S. and Nguyen, T. V. (1999). Multi-component transport in porous electrodes in proton exechange membrane fuel cells using the interdigitated gas distributors. *J. Electrochem. Soc.*, **146**, 38.

Yang, W. C. (2000). Fuel cell electric vehicle: Recent advances and challenges. *Int. J. Automotive Technology* **1**, **1**, 9–16.